Synergetic of Pt nanoparticles and H-ZSM-5 zeolites for efficient CO_2 activation: Role of interfacial sites in high activity

András Sápi[*,†], *Upendar Kashaboina*[†], *Kornélia B. Ábrahámné*[†], *Juan Fernando Gomez Perez*[†], *Imre Szenti*[†], *Gyula Halasi*[†], *János Kiss*[φ, Ψ], *Balázs Nagy*[†], *Tamás Varga*[†], *Ákos Kukovecz*[†,], *Zoltán Kónya*[†,Ψ]

[†]Department of Applied and Environmental Chemistry, University of Szeged, H-6720 Szeged, Hungary

[φ]Department of Physical Chemistry and Material Science, University of Szeged, H-6720 Szeged, Hungary

[Ψ]MTA-SZTE Reaction Kinetics and Surface Chemistry Research Group, University of Szeged, H-6720 Szeged, Hungary

[Φ]MTA-SZTE "Lendület" Porous Nanocomposites Research Group, University of Szeged, H-6720 Szeged, Hungary

Abstract: Catalytic systems prepared by controlled processes play an important role in the utilization of CO_2 via catalytic hydrogenation to produce useful C1 chemicals (such as CO, CH_4 and CH_3OH), which will be vital for forthcoming applications in energy conversion and storage. Size-controlled Pt nanoparticles were prepared by a polyol method and deposited on H-ZSM-5 (SiO_2/Al_2O_3 = 30, 80 and 280) zeolite supports. The prepared catalysts were tested for the CO_2 hydrogenation in the temperature range of T = 473–873 K and ambient pressure, with CO_2/H_2 = 1:4. Size-controlled Pt nanoparticles boosted the catalytic activity of the pure H-ZSM-5 zeolites resulted in ~16 times higher CO_2 consumption rate. The activity were ~4 times higher and CH_4 selectivity at 873 K was ~12 times higher over 0.5 % Pt/ H-ZSM-5 (SiO_2/Al_2O_3 = 30) compared to 0.5 % Pt/H-ZSM-5 (SiO_2/Al_2O_3 = 280). In-situ DRIFTS studies assuming the presence of a

surface complex in which the CO is perturbed by hydrogen and adsorbes via C-end on Pt but the oxygen tilts to the protons of the zeolite support.

Keywords: *Carbon dioxide; Hydrogenation; Platinum nanoparticles; ZSM-5*

*Corresponding Author
Telephone: +36-62-343-795;
E-mail addresses: sapia@chem.u-szeged.hu (A. Sápi).

1. Introduction

In recent decades, the industrialization and population growth have resulted in record high atmospheric concentration of greenhouse gases threatening the development of our economy and society[1,2]. At the same time, the dispute between the increasing energy requirement and declining non-renewable fossil fuel resources could cause a foreseeable crisis to mankind. Carbon dioxide (CO_2) is the second most abundant greenhouse gas after water vapor. The utilization of CO_2 as a C1 building block is an outstanding approach towards decreasing the global CO_2 emissions and additionally initiates a new sustainable direction for producing beneficial feedstock chemicals and fuels [3,4,5,6]. CO_2 is a thermodynamically stable molecule where the activation of CO_2 requires significant Gibbs energy input ($\Delta G°_{298.15}$ = -394.4 kJ·mol^{-1}). In the presence of H_2, the catalytic hydrogenation of CO_2 is a thermodynamically favorable reaction. However, the most important nature of the proposed catalyst for CO_2 conversion is that it should lower the activation energy barriers in the various reactions of CO_2 with H_2. The key reactions along with their enthalpy and Gibbs energy values are listed below.

Reverse water gas shift reaction (RWGS): $CO_2 + H_2 \rightarrow CO + H_2O \cdots\cdots\cdots (1)$

$$\Delta H_{298\,K} = 41.2\ kJ \times mol^{-1};\ \Delta G_{298\,K} = 28.6\ kJ \times mol^{-1}$$

CO_2 methanation: $CO_2 + 4H_2 \rightarrow CH_4 + 2H_2O \cdots\cdots\cdots\cdots\cdots\cdots\cdots\cdots\cdots\cdots\cdots\cdots (2)$

$$\Delta H_{298\,K} = -252.9\ kJ \times mol^{-1};\ \Delta G_{298\,K} = -113.5\ kJ \times mol^{-1}$$

Methanol formation: $CO_2 + 3H_2 \rightarrow CH_3OH + H_2O \cdots\cdots\cdots\cdots\cdots\cdots\cdots\cdots (3)$

$$\Delta H_{298\,K} = -49.5\ kJ \times mol^{-1};\ \Delta G_{298\,K} = 3.8\ kJ \times mol^{-1}$$

The catalytic hydrogenation of CO_2 to CO, known as the RWGS reaction (eq.1), is one of the promising ways to convert CO_2, whereas economize on the utilization of hydrogen compared with other CO_2 hydrogenation reactions[7]. In addition to that, the production of CO via RWGS reaction might be the best replacement technique to conventional coal gasification technology, which will become a basis for the future green coal chemistry industry. Particularly, methanation of CO_2 (eq. 2) is also one of the most significant reactions, this reaction can transform the exhausted CO_2 into methane (CH_4), where the formed methane can be recycled for the synthesis of fuel or chemicals [8,9].

Typically, ZSM-5 are used as sorbents and catalyst due to their unique channel structure, thermal stability, acidity, and shape-selective property [10,11]. Furthermore, the boosting effect of the size-controlled Pt nanoparticles (NPs) on the hydrogenation reaction of CO_2 was extensively studied and was attributed to the active cooperation of the metallic Pt and oxide support[12]. In this work, our purpose is to prove that the anchoring of Pt NPs on different ZSM-5 zeolite supports is a favorable heterogeneous hybrid catalyst for the hydrogenation of CO_2 into valuable products.

In their early work, Roman-Martinez and co-workers studied the structure sensitivity of Pt-based catalysts for the hydrogenation of CO_2[13]. Recently, Shyam *et al.* studied the effect of Pt interaction over different oxide (e.g. SiO_2, TiO_2, etc.) supports[14]. It was found that the formation of CO is preferred to that of $HCOO^-$ ion, both kinetically and thermodynamically, indicating that

methane can preferably be formed on the Pt-based catalysts. Therefore, when Pt NPs are packed on the zeolite support for hydrogenation of CO_2, the distribution of products is significantly affected due to the long contact time of reactant gases over the catalyst as well as the special pore structure of the zeolites. Particularly, the methanation process of CO_2 ($CO_2 \rightarrow CO \rightarrow CH_4$) involves the formation of CO as an intermediate and CH_4 as the final product. For this reason, constructions of such composites with Pt NPs would be advantageous to find the correlation between CO/CH_4 selectivity and structure sensitivity of the catalyst[15,16]. Zhan et al. also studied a novel sandwich type ZIF-67@Pt@$mSiO_2$ nanocube catalyst in CO_2 hydrogenation reaction[17]. It was reported that CO_2 hydrogenation on Na-modified, Fe-based Fischer-Tropsch catalyst[18] and In_2O_3 catalyst[19] combined with H-ZSM-5 exhibited excellent selectivity in gasoline, and a CeO_2−Pt@$mSiO_2$−Co tandem catalyst with two metal-oxide interfaces converted CO_2 to C2−C4 hydrocarbons with 60 % selectivity[20]. Very recently, Zheng et al. developed a highly active catalyst that is a monodispersed spherical Zr-based metal-organic framework catalyst, Pt/Au@Pd@UIO-66, comprising an Au@Pd core-shell encapsulated in a UIO-66 center for the hydrogenation of CO_2 [21].

In this study, 4.5 nm controlled-size Pt nanoparticles were anchored onto the surface of H-ZSM-5 zeolites with different Si/Al ratio and were tested in CO_2 hydrogenation reaction at 723-873 K. Size-controlled Pt nanoparticles boosted the catalytic activity of the pure H-ZSM-5 zeolites resulted in ~16 times higher CO_2 consumption rate. The activity was ~4 times higher and CH_4 selectivity at 873 K was ~12 times higher over 0.5 % Pt/ H-ZSM-5 (SiO_2/Al_2O_3 = 30) compared to 0.5 % Pt/H-ZSM-5 (SiO_2/Al_2O_3 = 280). In-situ DRIFTS studies assuming the presence of a surface complex in which the CO is perturbed by hydrogen and adsorbes via C-end on Pt but the oxygen tilts to the protons of the zeolite support.

2. Experimental Section

2.1. Synthesis of the H-ZSM-5 based catalysts for CO_2 hydrogenation reactions

2.1.1. Synthesis of the H-ZSM-5 zeolites

All NH_3-ZSM-5 zeolites were purchased from Alfa Aeasar. NH_3-ZSM-5-30 zeolite has a SiO_2:Al_2O_3 molar ratio of 30:1, NH_3-ZSM-5-80 zeolite has a SiO_2:Al_2O_3 molar ratio of 80:1 and NH_3-ZSM-5-280 zeolite has a SiO_2:Al_2O_3 molar ratio of 280:1. All the zeolites were calcined in air at ambient pressure and a temperature of 973 K for 5 hours before the investigation and heterogeneous catalytic tests to stabilize the protonated ZSM-5 form. We use the notation H-ZSM-5-30, H-ZSM-5-80, H-ZSM-5-280, respectively, to specify the various calcined zeolites according to their composition.

2.1.2. Synthesis of 4.4 ± 0.6 nm platinum nanoparticles

The following method was used for the preparation of 4.4 nm Pt nanoparticles. 41 mg H_2PtCl_4 and 20 mg polyvinylpyrrolidone (PVP, MW= 40.000) were dissolved in 5 ml ethylene-glycol and sonicated for 30 min to get a homogeneous solution. The solution was evacuated and purged with atmospheric pressure argon gas. After three purging cycles, the flask was immersed into an oil bath heated to 473 K under vigorous stirring of the reaction mixture as well as the oil bath. After 120 min of reaction, the flask was cooled down to room temperature. The suspension was precipitated by adding acetone to the mixture. After precipitation, the particles were washed by centrifugation with hexane and re-dispersing in ethanol.

2.1.3. Synthesis of 0.5 % Pt-H-ZSM-5 catalysts

To fabricate the supported catalysts, the proper amount of ethanol suspension of Pt nanoparticles with known Pt concentration (measured with ICP-MS) and the H-ZSM-5 zeolite with different

Si/Al ratio after calcination at 973 K were mixed together in ethanol and sonicated in an ultrasonic bath (40 kHz, 80 W) for 3 h. The supported nanoparticles were collected by centrifugation. The products were washed with ethanol three times and subsequently dried at 353 K overnight. H-ZSM-5-30, H-ZSM-5-80 and H-ZSM-5-280 zeolites loaded with Pt nanoparticles are labeled as Pt-H-ZSM-5-30, Pt-H-ZSM-5-80 and Pt-H-ZSM-5-280 according to their SiO_2/Al_2O_3 composition ratio.

2.2. Characterization of the ZSM-5 supports and Pt-H-ZSM-5 catalysts

The morphology of the support, as well as the dispersion of the Pt nanoparticles over the zeolite supports, was investigated by Transmission Electron Microscopy (TEM, FEI TECNAI G220 X-TWIN operated at 200 kV).

The crystal structure of the NH_3-ZSM-5, as well as the H-ZSM-5, were examined by X-ray Diffraction (XRD, Rigaku MiniFlex II Desktop Diffractometer operated with a Cu Kα source (λ= 0.1542 nm) at 30 kV and 15 mA).

The surface properties, specific surface area, and pore size distributions were investigated using a Quantachrome NOVA 3000e gas sorption instrument by N_2 adsorption at liquid N_2 temperature. The temperature-programmed desorption (TPD) was carried out in a BELCAT-A apparatus using a reactor (quartz tube with 9 mm outer diameter) that was externally heated. Before the measurements, the catalyst samples were treated in oxygen at 1073 K for 30 min. Thereafter, the sample was cooled in flowing Ar to room temperature and equilibrated for 15 min. The oxidized sample was flushed with Ar containing 10% H_2, and the reactor was heated linearly at a rate of 20 $K \cdot min^{-1}$ up to 1373 K. The H_2 consumption was detected by a thermal conductivity detector (TCD). The powders were first out-gassed at 473 K to ensure a clean surface.

Inductively coupled plasma (ICP) mass spectrometry was used for the determination of the metal content in each sample synthesized. The measurements were performed with an 'Agilent 7700x' type ICP-MS spectrometer. The sample was previously dissolved in an acidic mixture of HNO_3 and HCl.

In-situ infrared spectroscopy measurements were carried out with an 'Agilent Cary-670' FTIR spectrometer equipped with 'Harrick Praying Mantis' diffuse reflectance attachment. The sample holder had two BaF_2 windows in the infrared path. The spectrometer was purged with dry nitrogen. The spectrum of the pretreated catalyst was used as a background. At room temperature, a CO_2:H_2 molar ratio of 1:4 was introduced into the DRIFTS cell. The tubes were externally heated to avoid condensation. The catalyst was heated under the reaction feed linearly from room temperature to 773 K, with a heating rate of 20 $K \cdot min^{-1}$ and IR spectra were collected at 50 K intervals. All spectra were recorded between 4000 and 900 cm^{-1} at a resolution of 2 cm^{-1}. Typically, 32 scans were registered. Due to the short optical path within the DRIFTS cell, the contribution of the reactant gases was negligible, and from the gas phase products, only the most intense features were observable.

2.3. CO_2 hydrogenation reaction in the flow mode

The hydrogenation of CO_2 was conducted in a fixed-bed down tubular quartz flow reactor at atmospheric pressure. The reactor system was equipped with a programmable temperature controller. A mixture of CO_2/H_2 with a ratio of 1:4 used as the feed. Typically, the catalytic activity tests were carried out using 0.2 g of pelletized catalyst (typically round-shaped pellet with 13 mm diameter and 1-3 mm thickness are pressed) which was suspended between two quartz wool plugs in the reactor and the remaining vacant space was filled with quartz beads. Firstly, the catalyst was

pretreated with O_2 at 50 mL·min^{-1} at 573 K for 30 min, followed by in-situ reduction at the above temperature using H_2 flow for 30 min. Then the reactor was cooled down to 473 K and the reaction was tested in the temperature range of 473-873 K under a mixture of CO_2/H_2 with a ratio of 1:4 and a flow rate of 50 ml/min. The catalyst was heated with 20 K/min upto 873 K than for time-on-stream reaction the temperature was held for another 6 hours. Outlet gases were fed into a gas chromatograph (GC 4890D, Agilent) equipped with PORAPAK QS+ S column and the products were analyzed by TCD and FID (Supelco EQUITY -1). Argon was utilized as a carrier gas for the gas chromatograph and hydrogen and synthetic air were used for FID. CO_2 conversion (X_{CO_2}) and product selectivity (S_{prod}) towards to CO and CH_4 and C_2H_4 are defined as follows:

$$X_{CO_2} = \frac{nX_{CO_2},in - nX_{CO_2},out}{nX_{CO_2},in} \ldots\ldots\ldots (4)$$

$$S_{prod} = \frac{n_{prod,out} \times N_C}{nX_{CO_2}, in - nX_{CO_2}, out} \ldots\ldots\ldots (5)$$

3. RESULTS AND DISCUSSION

3.1. Structural and textual properties

In our characterization experiments, the Brunauer-Emmett-Teller (BET) gas adsorption method was used for the determination of surface area of the catalysts. Results for the BET surface area (S_{BET}), total pore volume (V_t) and pore radius are summarized in Table 1. The BET surface area, as well as the pore radius of H-ZSM-5 zeolites, are insensitive to the Si:Al ratio (330.4 – 360.3 $m^2 \cdot g^{-1}$, 1.93-1.95 A, respectively). However, the pore volume was ~2 times higher in the case of H-ZSM-5-30 zeolite compared to the other counterparts with higher Si/Al ratio.

Table 1: Parameters based on the N_2 adsorption measurements of the pure H-ZSM-5 zeolites with different SiO_2:Al_2O_3 ratio				
Catalyst	**S_{BET} (m^2/g)**	**V_m (cm^3/g)**	**Pore Radius (A)**	**V_t (cm^3/g)**
H-ZSM-5-30	330.4	0.133	1.93	0.24
H-ZSM-5-80	360.3	0.073	1.94	0.22
H-ZSM-5-280	350.0	0.063	1.95	0.22

S_{BET} is the BET specific surface area
V_m is the pore volume
V_t is the total specific pore volume calculated from the volume adsorbed of P/P_0 at 0.98 (the highest measuring point).
The N_2 adsorption-desorption method was used to find the specific surface area (S_{BET}) of the materials.

Nitrogen adsorption-desorption isotherms of H-ZSM-5 zeolites are presented in Figure 1. The hysteresis loop confirms the type-IV behavior (type H2 according to IUPAC classification) [22], which is related to capillary condensation taking place in the mesopores and also 3D interconnectivity of the pores. In the case of H-ZSM-5-30, the largest hysteresis loop was observed at high pressure which is attributed to the large internal void.

Typically, the catalytic hydrogenation of CO_2 depends upon the surface distribution of the acidic-basic sites of the materials. The Brønsted acidic sites can be essential for the activity in the field of catalysis[23] and most of these sites exist within the pore structure of the catalyst.

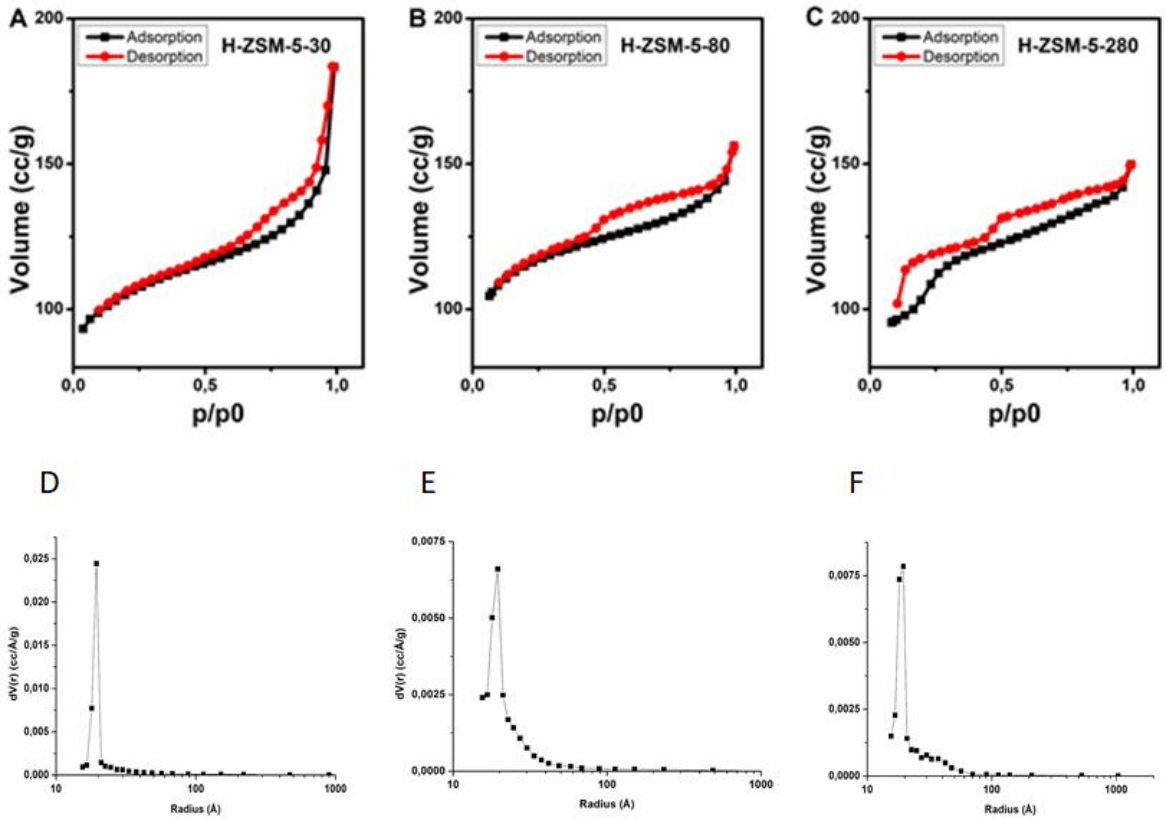

Figure 1: N_2 adsorption-desorption isotherm plot as well as the pore size distribution of the pure H-ZSM-5 zeolites.

In the case of the H-ZSM-5 zeolites, the total and Brønsted acidity of the catalysts were measured by TPD of ammonia and the resulted graphs are shown in Fig. 2/A. Table 2. represents the obtained values of the week and strong acidic sites (from figure 2/A.) and basic sites (from figure 2/B.). Two distinct NH_3 or NH^{4+} desorption peaks are observed in all H-ZSM-5 supports. The peaks at 454-481 K and 653-670 K corresponding to weak (physisorbed NH_3) and strongly-bonded Brønsted acid sites, respectively. In the case of the zeolites with lower Si/Al ratio, a higher amount of acidic sites were obtained. Costa et. al. already reported on the acidity of ZSM-5 zeolites, that the acidity depends on the Si/Al ratio and the number of the total acidic sites

decreased with the increasing Si/Al ratio[24]. The ammonium desorption peak temperature increases as the Si/Al ratio decreases. In the case of the weak acidic sites, the ammonia desorption takes place at 454 K, 476 K and 481 K for H-ZSM-5-280, H-ZSM-5-80 and H-ZSM-5-30, respectively. A similar trend was observed in the case of the strong acidic sites (H-ZSM-5-280: 653 K, H-ZSM-5-80: 678 K, H-ZSM-5-30: 670 K), however, the strength of the acidic sites for H-ZSM-5-80 and H-ZSM-5-30 are close to each other.

Thus, decreasing the Si/Al ratio the peak corresponding to the weak acidic sites was shifted to lower temperatures, indicating the decreasing strength of such acidic sites. The highest total amount of acid sites was obtained over the H-ZSM-5-30 zeolite (0.75 mmol $NH_3 \cdot g^{-1}$)[25] due to the lowest Si/Al ratio and the lowest total number of acidic sites was observed for H-ZSM-5-280 (0.12 mmol $NH_3 \cdot g^{-1}$) due to the high Si/Al ratio. On the other hand, the ratio of the strong/weak acidic sites is the lowest in the case of the H-ZSM-5-30 zeolite. In summary, in the case of the H-ZSM-5-30 support, NH_3-TPD study showed that the acidic site concentration of the zeolite surface, as well as the strength of the sites was the highest, while the distribution of the weak and strong sites showed the lowest ratio of strong/weak sites.

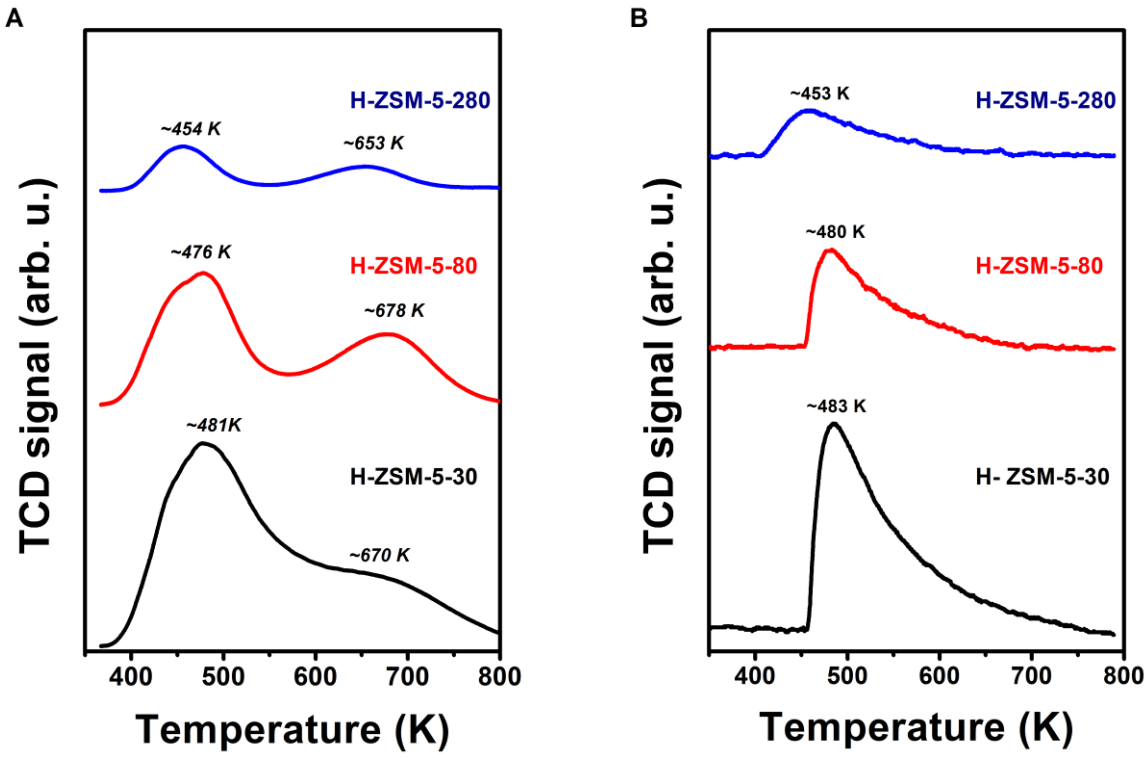

Figure 2: Temperature programmed desorption (TPD) of the H-ZSM-5 catalysts; (a) TPD of ammonia, (b) TPD of CO_2.

Figure 2/B. represents the TPD-CO_2 profiles for the various H-ZSM-5 supports. The CO_2 adsorption capacity was the highest for H-ZSM-5-30 and the lowest for H-ZSM-5-280 with the value of 0.167 mmol $CO_2 \cdot g^{-1}$ and 0.041 mmol $CO_2 \cdot g^{-1}$, respectively. Also, the CO_2 desorption temperature is the highest for H-ZSM-5-30. From these results, we can conclude that H-ZSM-5-30 has the strongest basic sites as well as the highest surface concentration of them compared to other H-ZSM-5 zeolites.

Table 2: Acidity and basicity of NH_3-ZSM-5 catalysts.

Catalyst	Acidity (mmol $NH_3 \cdot g^{-1}$)						Basicity (mmol $CO_2 \cdot g^{-1}$)
	Weak	T (K)	Strong	T (K)	Total	Strong/weak	
H-ZSM-5-30	0.53	481	0.22	670	0.75	0.42	0.167
H-ZSM-5-80	0.26	476	0.20	678	0.46	0.77	0.073
H-ZSM-5-280	0.065	454	0.056	653	0.121	0.86	0.041

N_2, NH_3 and CO_2 adsorption/desorption studies are bringing the following conclusions useful for our system as well as catalytic behavior. The Pt NP dispersion on the surface of the H-ZSM-5 supports may depend on the acidic strength of the support: the more acidic is the surface, the less sintering during the reaction maybe expected. However, earlier studies showed that Pt nanoparticles with > 5 nm sizes are not showing any sintering under similar reaction conditions[33]. It is worth mentioning that the lack of the Brønsted acidic sites over the zeolite supports, the Pt NPs are not stable and consequently might be leading to the formation of their agglomeration over the support. Therefore, high acidic and also more basic zeolites (here: NH_3-ZSM-5-30) may offer higher stability for Pt species as well as different interfacial metal–support interactions[26]. The above trend should be described through the following way; the Pt atom coordinated with a Brønsted proton and with a nearby bridging framework oxygen in the ZSM-5 support. These metal-support interacted sites are good for adsorption of CO_2 and may also offer CO_2 activation leads to higher catalytic activity as well as selectivity towards the desired products.

X-ray diffraction (XRD) patterns of the pure supports are displayed in Fig. 3. Almost all NH_3-ZSM-5 samples are exhibited the similar diffraction patterns at 2θ angles of 7.9º, 8.8º, 23.1º and 23.7°, which represent the (011), (020), (051) and (033) planes, respectively,[27] characteristic for ZSM-5 type zeolites. The insignificant differences between NH_3-ZSM-5-30 and H-ZSM-5-30

samples show that the heat treatment of the samples at 973 K has no effect on the structure of zeolites. On the other hand, we can conclude that the structure of ZSM-5 remains intact at all Si/Al ratio.

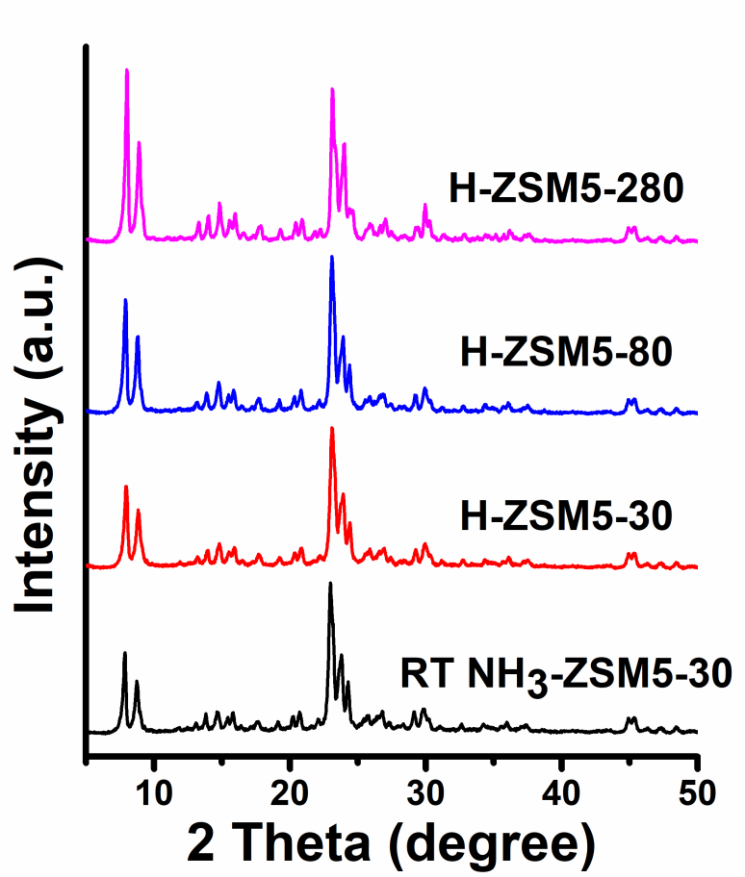

Figure 3: XRD patterns of the NH_3-ZSM-5 catalysts.

Figure 4 shows the TEM images of the Pt-NH_3-ZSM-5 catalysts presented in this study. It is important to say that the polyol based method of Pt nanoparticle synthesis resulted incontrolled-size nanoparticles with a narrow size distribution centered at 4.4 ± 0.6 nm, where the particles have a spherical shape.

The Pt nanoparticles were uniformly dispersed on the H-ZSM-5 zeolites in all three Si/Al ratio cases. The microporous nature and the surface acidity of the ZSM-5 support helps the adsorption of Pt nanoparticles, which in turn improves the interaction between the Pt nanoparticles and the H-ZSM-5 zeolites which also resulted in the development of isolated and well-dispersed Pt nanoparticles on the surface.

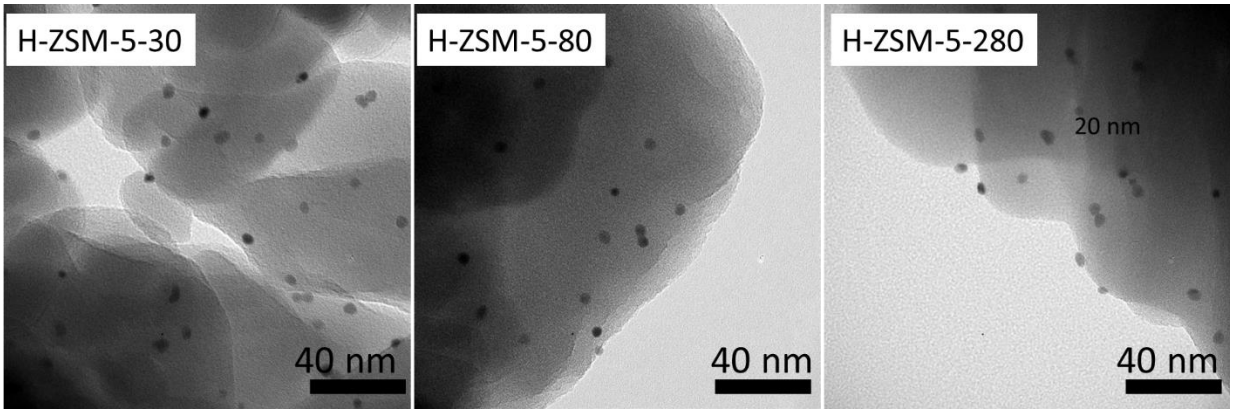

Figure 4: TEM images of H-ZSM-5 zeolite supported 4.4 nm Pt nanoparticles

3.2. Catalytic Hydrogenation of CO_2

H-ZSM-5 catalysts with different Si/Al ratios (30, 80 and 280) as well as their counterparts loaded with 0.5% of 4.4 nm Pt nanoparticles were tested in CO_2 hydrogenation reaction in a flow reactor in the temperature range of 473 K – 873 K at ambient pressure. Before the catalytic tests, the catalysts were pretreated in O_2 at 573 K followed by H_2 reduction at the same temperature.

Initially, Pt-free H-ZSM-5 supports were tested where we found that the catalysts have slight activity at 723-873 K where the main products were CO, CH_4 as well as C_2H_4 (Figure 6.). Zeolite with the highest aluminum content (H-ZSM-5-30) showed the highest catalytic activity compared to H-ZSM-5-80 and H-ZSM-5-280 at 723 K. In the case of the H-ZSM-5-80, the lowest catalytic activity was observed. In the case of H-ZSM-5-280, the highest catalytic activity (120

nmol·g^{-1}·s^{-1}) was observed at 873 K, which was ~2 times higher compared to the activity of H-ZSM-5-30 and that of H-ZSM-5-80. The catalytic activity was 5 times higher in the case of H-ZSM-5-280 at 873 K compared to the activity at 723 K. While catalytic activity was increased in the case of the H-ZSM-5-30 at higher temperature, the increment was not as significant. These unusual phenomena maybe attributed to the investigation at the low conversion regime, as well as the special influence of the different ratio of the weak and strong acidic sites as well as the basic sites developed by NH_3-TPD and CO_2-TPD under these low activity range.

In the case of the Pt-free zeolites, CO, CH_4, and C_2H_4 were formed at 723 K, while only CO and CH_4 was observed at 873 K. H-ZSM-5-280 showed the highest selectivity towards CH_4 (80%) at 723 K compared to H-ZSM-5-30 (2%) and H-ZSM-5-80 (62%). H-ZSM-5-30 produced 100% while there was no CO in the case of H-ZSM-5-80 and H-ZSM-5-280. A significant amount of C_2H_4 was formed in the case of H-ZSM-5-80 (36%) and H-ZSM-5-280 (22 %).

At 873 K, CO was the main product in case of the testing of all Pt-free zeolites. While the formation of CH_4 is insignificant, it was observed that H-ZSM-5-80 showed the highest CH_4 selectivity (0,7%) compared to H-ZSM-5-30 (0,25 %) and H-ZSM-5-280 (0,2 %).

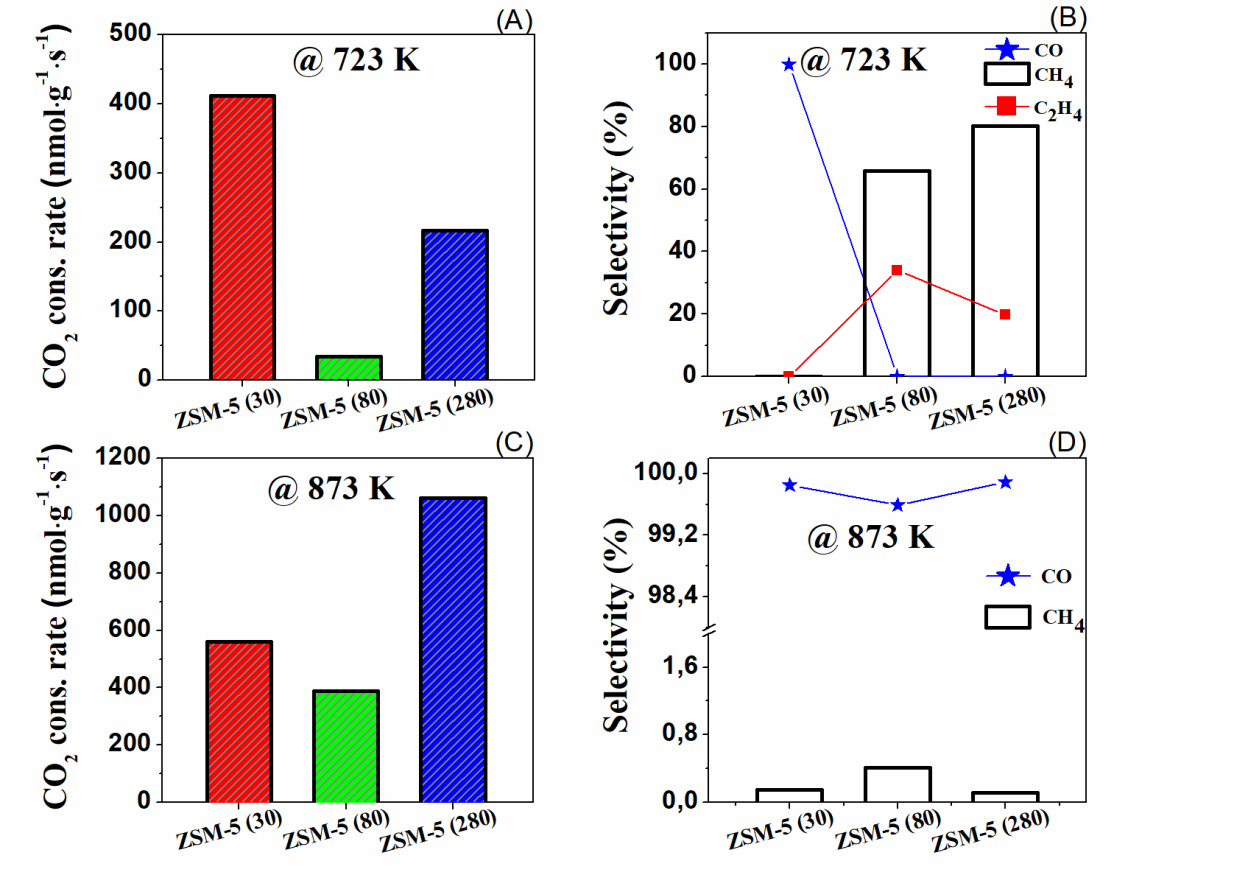

Figure 6: CO_2 Consumption rate and distribution of products at 723 K and 873 K over Pt-free, H-ZSM-5 zeolites.

4.4 nm Pt nanoparticles anchored to the surface of the different H-ZSM-5 catalysts were also tested in CO_2 hydrogenation reactions (Figure 7.). H-ZSM-5-30 were able to consume CO_2 with a rate of 410 mmol·g^{-1}·s^{-1} and 580 mmol·g^{-1}·s^{-1} at temperatures of 723 K and 873 K, respectively. the consumption rate of CO_2 was enormously increased after the addition of Pt nanoparticles (i.e. Pt-H-ZSM-5-30 performed with a CO_2 consumption rate of 1630 mmol·g^{-1}·s^{-1} and 8130 mmol·g^{-1}·s^{-1} at 723 K and 873 K, respectively). Pt supported on zeolites with lower Si/Al ratio showed higher activity. In the case of Pt-H-ZSM-5-30, the catalytic activity (1630 mmol·g^{-1}·s^{-1}) was 3 times as well as 4 times higher compared to the activity of Pt-H-ZSM-5-80 (530

mmol·g^{-1}·s^{-1}) and Pt-H-ZSM-5-280 (460 mmol·g^{-1}·s^{-1}), respectively at 723 K. The same trend was observed in the case of activity at 873 K.

For the Pt-H-ZSM-5 catalysts CO and CH_4 was the main product, where a small amount of C_2H_4 was formed only at 723 K. All the Pt-loaded catalysts were more selective to CO than CH_4 at 723 K as well as 873 K. The CH_4 selectivity is low, however, the Pt-H-ZSM-5-30 catalysts show 3-10 times higher methane selectivity compared to the catalysts based on zeolites with higher Si:Al ratio. At 873 K, in the case of the Pt-H-ZSM-5-30 catalyst, the methane selectivity is 20 times higher compared to the Pt-free, H-ZSM-5-30 zeolites.

After we tested the samples upto 873 K, the catalysts were monitored at the same temperature for another 6 hours. During the time-on-stream measurements no significant deactivation was observed.

Anchoring of Pt NPs over the H-ZSM-5 zeolites directed to the synthesis of a more active catalyst, where the pores of the zeolite support are appropriate to adsorb the reactant molecules (CO_2 and H_2). Presumably, the Pt NPs are located on the surface as well as in the channels of the zeolites support and the upcoming CO_2 can be captured inside the cage. Then the concentration of CO_2 is much higher near the Pt NP. It is worth mentioning that with increasing the reaction temperature, the methane (hydrocarbon) selectivity decreased and the CO selectivity increased. Therefore, we deliberate that the relatively lower temperature is suitable for obtaining a high yield of methane. The superior performance of Pt-H-ZSM-5-30 can be attributed to its highest Brønsted acidity but also to the formation of homogeneously dispersed Pt NPs over the zeolite support. The resultant composite catalysts are highly active in gas-phase CO_2 hydrogenation, in which the reaction pathway involves (i) a Pt site that might be involved in the formation of CO from CO_2 through the reverse water gas shift reaction and, subsequently, (ii) methanation and or

hydrogenation of CO catalyzed by the nearby Brønsted acidic sites. This can be explained by the following way; the edges and corners of the Pt nanoparticles are active sites and kinetically preferred to stimulate the hydrogenation of the CO_2 reaction. The adsorption of CO_2 over the Pt NPs (binding energy = − 0.23 eV) is the rate-determining step for the overall conversion of CO_2 to CO, CH_4, CH_3OH, and C_2H_4. For a deeper understanding of the mechanisms, high activity and behavior of the catalysts in-situ DRIFTS studies were performed and discussed in the following section.

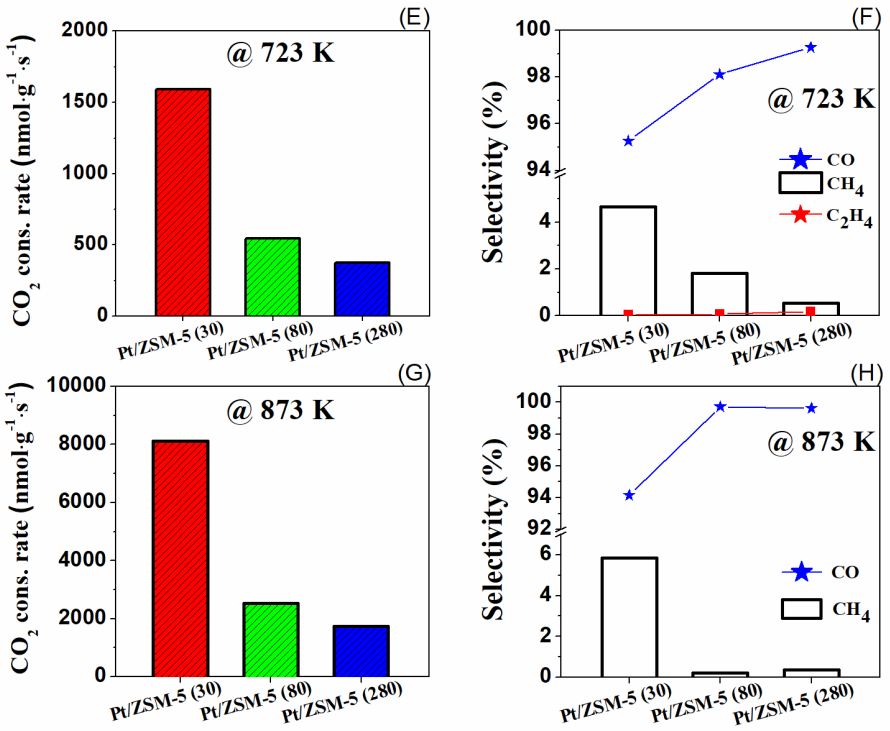

Figure 7: CO_2 Consumption rate and distribution of products at 723 K and 873 K over 0.5 % Pt supported on H-ZSM-5 catalysts.

3.2.1. In-situ DRIFTS Studies of the catalysts under reaction conditions

For heterogeneous catalytic reactions, the exploration of surface species formed during the catalytic processes plays a decisive role in understanding the reaction mechanism. Towards this goal, DRIFT spectra were monitored at increasing reaction temperatures, in the presence of the reactant mixture/products. The detailed infrared studies were performed on H-ZSM-5-30 for reference state, as well as on Pt-H-ZSM-5-30 and Pt-H-ZSM-5-280 catalysts under reaction conditions (4:1 H_2:CO_2 ratio at 323 – 773 K) using FTIR spectrometer equipped with diffuse reflectance attachment (Figure 8, 9).

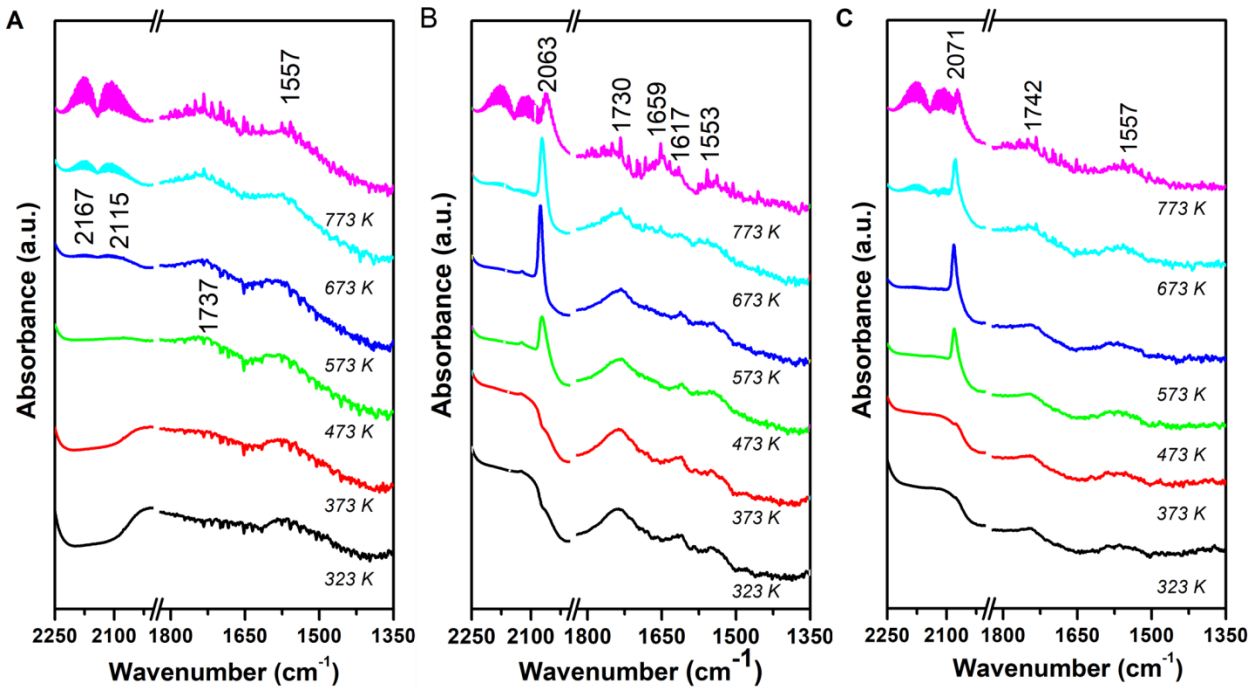

Figure 8. DRIFTS spectra of H-ZSM-5-30 (A), Pt-H-ZSM-5-30 (B) and Pt-H-ZSM-5-280 (C) under reaction conditions (CO2:H2 = 1:4) at 323 – 773 K

The evaluation of the low wavenumber (1300-2000 cm^{-1}) region is difficult, as the zeolites itself has weak absorptions at the region as well as a sharp absorption edge at ~1300 cm^{-1}. Although these features should be accounted for by the background spectrum, they might also change as a function of temperature and thus disturb our spectra. Above the frame vibrations of zeolites we obtained relatively weak bands at 1557 cm^{-1} already at 323 K in the case of H-ZSM-5-20 (Figure 8A). These bands can be attributed to the formation of formate ion ($HCOO^-$) from the CO_2 + H_2 reaction mixture, and these are assigned to ν_a(OCO) and ν_s(OCO) vibrations, respectively.[31,32,32]. When the reaction temperature is increased to 573 K, a new weak peak developed at 1737 cm^{-1} which can be tentatively assigned to aldehyde like CO stretch[33,34]. These bands were present up to 873 K, from 673 K peaks for gas phase CO (2115 and 2167 cm^{-1}) and methane (3013 cm^{-1}) showed up (not shown here). It is interesting that when the acidity is decreased by the increasing Si/Al ratio, the formaldehyde-like CO (formyl) decreases, on the surface of Pt-H-ZSM-5-280.

It is very likely, in line with the literature data obtained on different catalysts[33,35,36] that the activation of CO_2 on zeolites does not occur basically via direct dissociation to adsorbed CO and O; rather it proceeds through a carboxylate or bicarbonate intermediate, which reacts with adsorbed hydrogen species and formate is produced[33,35]. The formate intermediate may transform to the formaldehyde form at higher temperatures if a significant number of protons are available:

$$CO_{2(a)}{}^{*} + H_{(a)}\,(OH_{(a)}) \rightarrow (HCO_3^-) \rightarrow HCOO_{(a)} + O_{(a)} \qquad (1)$$

$$HCOO_{(a)} + H_{(a)} \rightarrow H_2CO_{(a)} \qquad (2)$$

On the other hand, the formate may decompose to methane[13] or CO as was observed on NiO[33], and at higher temperatures, the formaldehyde may transform to gas phase CO on TiO_2[31]:

$$H_2CO_{(a)} \rightarrow CO_{(g)} + 2H_{(a)} \qquad (3)$$

On Pt free zeolites the reaction partway strongly depends on acidity and, in harmony with this, on the Si/Al ratio. On less acidity sample this kind of formaldehyde form was not observed on IR spectra. According to catalytic measurements on pure zeolite CO formation was the significant reaction pathway. We may suppose that the CO formation occurs via decomposition of formate:

$$HCOO_{(a)} \rightarrow CO_{(a)} + OH_{(a} \qquad (4)$$

At the high Si/Al ratio with less acidic character, the formate may partially decompose via C-O bond breaking and the CH fragments hydrogenate to methane according to RWGS reaction[37]

$$HCOO_{(a)} \rightarrow H_2COH_{(a)} \rightarrow H_2C_{(a)} + OH_{(a)} \qquad (5)$$

$$H_2C_{(a)} + 2H_{(a)} \rightarrow CH_{4(g)} \qquad (6)$$

Ethylene formation was also detected on zeolites with less acidic character (Figure 6B). It means that a certain fragment of $CH_{2(a)}$ recombines, and ethylene is formed in a fast coupling reaction step:[38]

$$H_2C_{(a)} + CH_{2(a)} \rightarrow C_2H_{4(g)} \qquad (7)$$

Adsorbed ethylene or ethylidine were not detected in DRIFTS during the reaction, it means that the ethylene forms in the surface reaction rate determine step.

Pt-H-ZSM-5-30 and Pt-H-ZSM-5-280 catalysts contain more absorption bands during the reaction (Figure 8/B,C). Peaks for bidentate formate also appeared at 1553 cm^{-1}, but unfortunately, the symmetric component probably overlaps with the Si-O stretching band. At low-temperature regime (323-573 K) a peak was detected at 1617 cm^{-1} wich is attributed to monodentate formate[35]

on Pt-H-ZSM-5-30. This peak may have a bicarbonate component which is the precursor for formate formation[35]. Formate species is generally accepted as a key intermediate in CO_2 hydrogenation in literature among others on Pt/NiO[33], Pd/Al_2O_3[35,39], Rh/Al_2O_3[40] and Rh/TiO_2.[34] We believe that in our case the bidentate form appears on the H-ZSM-5 and monodentate formate on the Pt sites which play also significant role in $CO_2 + H_2$ reaction. As we demonstrated in Fig. 7/B, the formation of methane drastically increased on Pt containing Pt-H-ZSM-5-30. The methane formation proceeds very probably through formate pathway[33,35,41] , preferentially on Pt sites:

$$HCOO_{(a)} + H_{(a)} \rightarrow HCOOH_{(a)}^{*} \qquad (8)$$

$$HCOOH^{*} + H_{(a)} \rightarrow H_2COOH_{(a)}^{*} \qquad (9)$$

$$H_2COOH_{(a)}^{*} \rightarrow H_nCO_{(a)}^{*} + OH_{(a)} \qquad (10)$$

The $H_nCO_{(a)}^{*}$ (n= 1,2) intermediates may stabilize on the surface either as adsorbed formaldehyde and decomposes to CO (equation 3) or decomposes to CH_2 via C-O rupture as it described in equations 5,6 and finally CH_4 was produced. Carbonyl hydrites, $H_nCO_{(a)}^{*}$ (n= 1,2) or with other words hydrogen perturbed adsorbed CO is frequently supposed in CO_2 hydrogenation reactions [35,42–44]. This band is usually detected at 1825-1840 cm^{-1}. In this structure, it is suggested that CO bonds linearly to noble metal perturbed by hydrogen[42,43]. The frequency shift (~200 cm^{-1}) comparing to simple linearly bond CO (2070 cm^{-1}) indicates a weakening in C-O bond. The support for hydrogen-assisted dissociation of CO comes from the observation of methane formation at temperatures lower than those required for dissociation in the absence of hydrogen[45]. BOC-MP calculation has also shown that the dissociation of H_nCO, where n=1,2, or 3, is energetically more favorable than the direct dissociation of CO on Pd or Pt[46]. We did not detect

this wavenumber but we observed further frequency shift in C-O bond (1730 cm^{-1}) even at 323 K (Fig. 8/B.), which indicates a further weakening in C-O bond.

The peak at 1730 cm^{-1} position may attributable to adsorbed formyl or formaldehyde (CH_2CO) as it was observed on Pt free H-ZSM-5-30 at high temperatures (Fig. 8A). However, we think that $H_nCO_{(a)}^*$ intermediate could also exist at this wavenumber on Pt-H-ZSM-5-30 from 323 K (Fig. 8B). For identification of this species, we should mention that band around 1750 cm^{-1} was observed upon CO adsorption on Co_3O_4(111) film (and at somewhat lower wavenumber on MgO(100) and Fe_3O_4(111)). The band was attributed to a weakly bound bidentate carbonate which is formed at defect site[47]. However, in our case, this band was not observed during adsorption of CO_2 without hydrogen. We suggest that the CO in this form exists in a surface complex in which the CO is perturbed by hydrogen and adsorbes via C-end on Pt but the oxygen tilts to the proton in zeolites. The other scenario is also imaginable; namely the $H_nCO_{(a)}^*$ bond to zeolite frame and the oxygen tilts to Pt site or hydrogen located on Pt at the interface. These two scenarios are shown in Figure 9. Recently, 1720 cm^{-1} infrared band was observed during the interaction of CO_2 with H_2 on Rh/Al_2O_3[x]. This band was attributed to bridge bonded CO species positioned between Rh and Al atoms from the support. In our study, in the case of the Pt-H-ZSM-5-30, the peak area of the 1737 cm^{-1} band decreases (Figure 10A) while CH_x and CH_3 species were developed with increasing temperature as well as >600 K gas phase methane was detected (Figure 10C). However, in the case of Pt-free H-ZSM-5-30, no CO or CH_x was detected only the presence of CH4 at elevated temperature (Figure 10B). This phenomena maybe attributed to the fact that, the inclined H-CO species is forming methane at the Pt/H-ZSM-5 interface, however, in the case of the Pt-free catalyst the formate route is favorable.

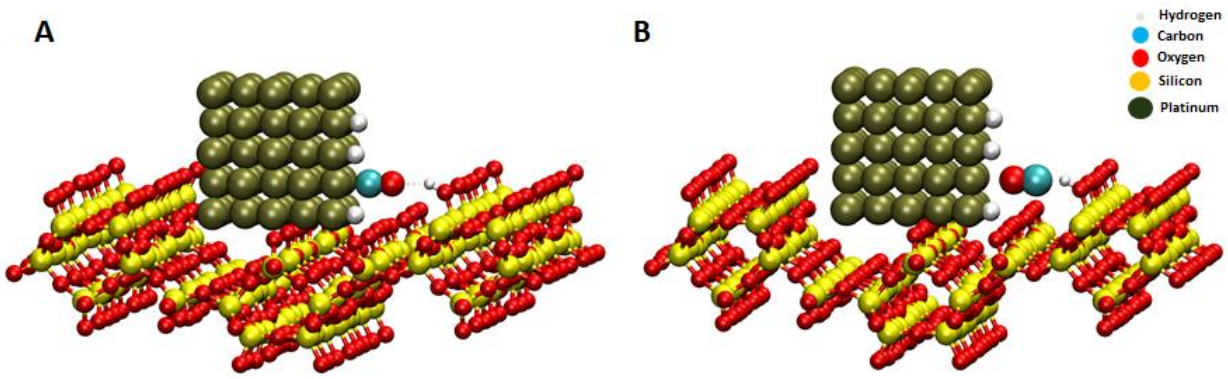

Figure 9. CO adsporbs on the Pt NP via the C end (A), and CO adsorbs to Pt NP via the O end (B)

The inclined, bent configuration plausibly significantly weakens the C-O bond (shifted further to lower wavenumbers) and it could easily break. Low wave number CO (1770 cm^{-1}) was detected under the reaction of $CO_2 + H_2$ on Rh supported on titanates[48]. In addition, this unusually low wave number was also observed in CO adsorption on Mn, La, Ce, Fe promoted Rh/SiO_2[49–51]. It was suggested that the oxygen on CO inclined to promoter cations, and enhanced the rupture of C-O bond. On Pt-containing most acidic ZSM-5 we suggest the following further steps in CO_2 hydrogenation (methane formation) where plenty of adsorbed hydrogen is available:

$$H_n(CO)_{(a)}\, H_{(a)} \rightarrow CH_{n\,(a)} + OH_{(a)} \qquad (11)$$

$$OH_{(a)} + H_{(a)} \rightarrow H_2O_{(g)} \qquad (12)$$

On Pt-containing zeolites ethylene formation was not observed (Fig. 7B), which means that the formed CH species does not recombine but reacts with hydrogen forming methane or further dehydrogenates where carbon is formed causing the deactivation of the catalysts:

$$CH_{n\,(a)} + H_{(a)} \rightarrow CH_{4(g)} \qquad (13)$$

$$CH_{n\,(a)} \rightarrow C_{(a)} + nH_{(a)} \qquad (14)$$

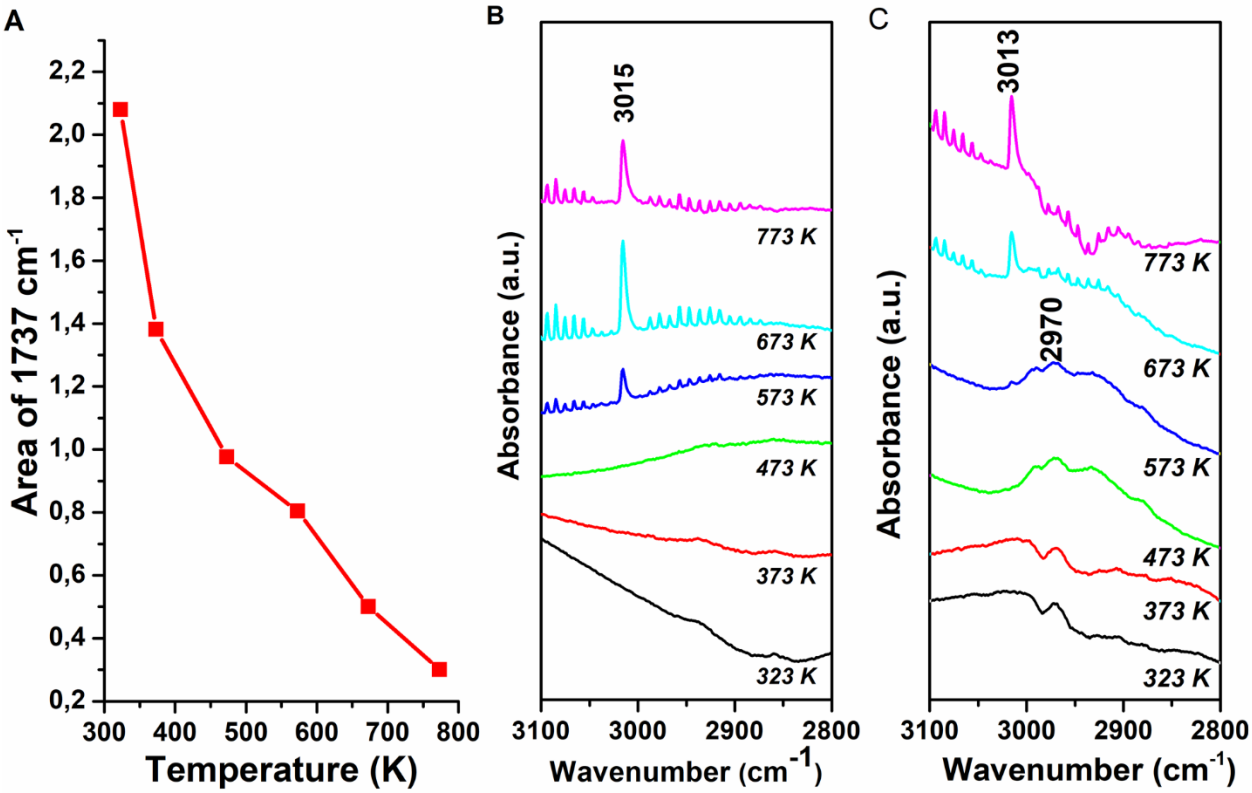

Figure 10. Peak area of the 1737 cm^{-1} peak region as a function of temperature (A), DRIFTS spectra of H-ZSM-5-30 in CH region (B), DRIFTS spectra of Pt-H-ZSM-5-30 in CH region during reaction condition (C).

The inclined CO has different structure and stability than that of the linearly adsorbed CO on Pt sites, which appeared at 2070 cm^{-1} (Fig. 8/B,C) from 573 K. It forms in formate decomposition or in reaction with hydrogen besides formaldehyde/formyl decomposition:

$$HCOO_{(a)} + H_{a)} \rightarrow CO_{(a)} + H_2O \qquad (15)$$

The other possible scenario is that CO_2 activated and forms adsorbed CO on Pt sites even at 300 K. This activation process proceeds via formation of negatively charged CO_2 radical and it converts to CO with the help of activated hydrogen[43,44, x].

The formed adsorbed CO starts to desorb above 600 K. The observed CO position is almost agreed with those detected on Pt-H-ZSM-5[52] previously. In that study two bands appeared; one is at 2095 cm^{-1}, the other is at 2080-2050 cm^{-1}. This later peak is ascribed to smaller Pt particles for which CO adsorbs abundantly on less coordinated Pt atoms. The peak at ~1730 cm^{-1} (formaldehyde and hydrogen perturbed inclined CO) is present up to 700-800 K. Above 773 K bands appeared at 1659 cm^{-1} probably due to carbonate which comes from the decomposition of formate and formaldehyde.

4. Conclusion

In summary, we synthesized 4.4 nm Pt nanoparticles with narrow size distribution and these Pt NPs were successfully anchored onto the surfaces of H-ZSM-5 (Si/Al= 30, 80 and 280) supports. The final composite catalysts are firstly explored for the hydrogenation CO_2 at 723 and 873 K temperatures and atmospheric pressure. The characterization results revealed that Pt NPs diffused H-ZSM-5 catalysts have been conceded for its unique property which makes potential candidates for catalytic hydrogenation of CO_2. Comparison with bare H-ZSM-5 catalysts the Pt NP modified composites showed superior catalytic activity. The lower Si/Al ratio composite was showing the highest catalytic activity. The reasons for this high activity as well as CH4 selectivity of 0.5 % Pt-H-ZSM-5-30 could be explained by the presence of the CO in a surface complex in which the CO is perturbed by hydrogen and adsorbes via C-end on Pt but the oxygen tilts to proton in zeolites The other scenario is also imaginable; namely the $H_nCO_{(a)}^*$ bond to zeolite frame and the oxygen tilts to Pt site or hydrogen located on Pt at the interface, where this inclined, bent

configuration plausibly significantly weakens the C-O bond being responsible for the high activity and selectivity of methane.

Acknowledgment

UK thank to the University of Szeged, Hungary, for the financial support. This paper was supported by the Hungarian Research Development and Innovation Office through grants NKFIH OTKA PD 120877 of AS. ÁK, GH and KZ is grateful for the fund of NKFIH (OTKA) K112531 & NN110676, PD 115769 and K120115, respectively. This collaborative research was partially supported by the "Széchenyi 2020" program in the framework of GINOP-2.3.2-15-2016-00013 "Intelligent materials based on functional surfaces – from syntheses to applications" project.

References

1. *International Energy Outlook 2013*. (U.S. Energy Information Agency, 2013). doi:EIA-0484(2013)

2. Mikkelsen, M., Jørgensen, M. & Krebs, F. C. The teraton challenge. A review of fixation and transformation of carbon dioxide. *Energy Environ. Sci.* **3,** 43–81 (2010).

3. Aresta, M., Dibenedetto, A. & Quaranta, E. State of the art and perspectives in catalytic processes for CO2 conversion into chemicals and fuels: The distinctive contribution of chemical catalysis and biotechnology. *J. Catal.* **343,** 2–45 (2016).

4. Wang, X. *et al.* Synthesis of isoalkanes over a core (Fe–Zn–Zr)–shell (zeolite) catalyst by CO_2 hydrogenation. *Chem. Commun.* **52,** 7352–7355 (2016).

5. Li, S. *et al.* Tuning the Selectivity of Catalytic Carbon Dioxide Hydrogenation over Iridium/Cerium Oxide Catalysts with a Strong Metal-Support Interaction. *Angew. Chemie Int. Ed.* **56,** 10761–10765 (2017).

6. Robert, M. Running the Clock: CO_2 Catalysis in the Age of Anthropocene. *ACS Energy Lett.* **1,** 281–282 (2016).

7. Danjun, W., Furong, T. a O., Huahua, Z., Huanling, S. & Lingjun, C. Preparation of Cu/ZnO/Al2O3 Catalyst for CO2 Hydrogenation to Methanol by CO2 Assisted Aging. *Chinese J. Catal.* **32,** 1452–1456 (2011).

8. Sakakura, T., Choi, J.-C. & Yasuda, H. Transformation of Carbon Dioxide. *Chem. Rev.* **107,** 2365–2387 (2007).

9. Olah, G. A., Goeppert, A. & Prakash, G. K. S. Beyond Oil and Gas: The Methanol Economy: Second Edition. *Beyond Oil Gas Methanol Econ. Second Ed.* 1–334 (2009). doi:10.1002/9783527627806

10. Falamaki, C., Edrissi, M. & Sohrabi, M. Studies on the Crystallization Kinetics of Zeolite ZSM-5 With 1,6-Hexanediol as a Structure-Directing Agent. *Zeolites* **19,** 2–5 (1997).

11. Kumar, N. *et al.* Effect of synthesis time and mode of stirring on physico-chemical and catalytic properties of ZSM-5 zeolite catalysts. *Appl. Catal. A Gen.* **235,** 113–123 (2002).

12. Sápi, A. *et al.* In-situ DRIFTS and NAP-XPS Exploration of the Complexity of CO2 Hydrogenation over Size Controlled Pt Nanoparticles Supported on Mesoporous NiO. *j. phys. chem. c* **122,** 5553-5565 (2018).

13. Román-Martínez, M. C., Carzorla-Amorós, D., Salinas-Martínez de Lecea, C. & Linares-

Solano, A. Structure Sensitivity of CO 2 Hydrogenation Reaction Catalyzed by Pt / Carbon Catalysts. *Langmuir* **12,** 379–385 (1996).

14. Kattel, S., Yan, B., Chen, J. G. & Liu, P. *CO 2 hydrogenation on Pt, Pt/SiO2 and Pt/TiO2 : Importance of synergy between Pt and oxide support*. *Journal of Catalysis* **343,** 115-126 (2016).

15. An, X., Zuo, Y.-Z., Zhang, Q., Wang, D. & Wang, J.-F. Dimethyl Ether Synthesis from CO 2 Hydrogenation on a CuO−ZnO−Al 2 O 3 −ZrO 2 /HZSM-5 Bifunctional Catalyst. *Ind. Eng. Chem. Res.* **47,** 6547–6554 (2008).

16. Takeguchi, T., Yanagisawa, K., Inui, T. & Inoue, M. Effect of the property of solid acid upon syngas-to-dimethyl ether conversion on the hybrid catalysts composed of Cu–Zn–Ga and solid acids. *Appl. Catal. A Gen.* **192,** 201–209 (2000).

17. Zhan, G. & Zeng, H. C. ZIF-67-Derived Nanoreactors for Controlling Product Selectivity in CO2Hydrogenation. *ACS Catal.* **7,** 7509–7519 (2017).

18. Wei, J. *et al.* Directly converting CO2 into a gasoline fuel. *Nat. Commun.* **8,** 15174 (2017).

19. Gao, P. *et al.* Direct conversion of CO2 into liquid fuels with high selectivity over a bifunctional catalyst. *Nat. Chem.* 1–26 (2017). doi:10.1038/nchem.2794

20. Xie, C. *et al.* Tandem Catalysis for CO_2 Hydrogenation to C_2–C_4 Hydrocarbons. *Nano Lett.* **17,** 3798–3802 (2017).

21. Zheng, Z., Xu, H., Xu, Z. & Ge, J. A Monodispersed Spherical Zr-Based Metal-Organic Framework Catalyst, Pt/Au@Pd@UIO-66, Comprising an Au@Pd Core-Shell

Encapsulated in a UIO-66 Center and Its Highly Selective CO2 Hydrogenation to Produce CO. *Small* **1702812,** 1–8 (2017).

22. Sing, K. S. W. *et al.* INTERNATIONAL UNION OF PURE COMMISSION ON COLLOID AND SURFACE CHEMISTRY INCLUDING CATALYSIS-Reporting physisorption data for gas/solid systems with special reference to the determination of surface area and porosity. *Pure Appl. Chem.* **57,** 603–619 (1985).

23. Zhao, Y. X., Bamwenda, G. R., Groten, W. A. & Wojciechowski, B. W. The Chain Mechanism in Catalytic Cracking: The Kinetics of 2-Methylpentane Cracking. *J. Catal.* **140,** 243–261 (1993).

24. Costa, C., Dzikh, I. P., Lopes, J. M., Lemos, F. & Ribeiro, F. R. Activity-acidity relationship in zeolite ZSM-5. Application of Bronsted- type equations. *J. Mol. Catal. A Chem.* **154,** 193–201 (2000).

25. Kim, Y. T., Jung, K. D. & Park, E. D. Gas-phase dehydration of glycerol over silica-alumina catalysts. *Appl. Catal. B Environ.* **107,** 177–187 (2011).

26. O'Malley, A. J. *et al.* Room temperature methoxylation in zeolites: insight into a key step of the methanol-to-hydrocarbons process. *Chem. Commun. (Camb).* **52,** 2897–2900 (2015).

27. Bin, F. *et al.* Selective catalytic reduction of nitric oxide with ammonia over zirconium-doped copper/ZSM-5 catalysts. *Appl. Catal. B Environ.* **150–151,** 532–543 (2014).

28. Ismail, A. A., Mohamed, R. M., Fouad, O. A. & Ibrahim, I. A. Synthesis of nanosized ZSM-5 using different alumina sources. *Cryst. Res. Technol.* **41,** 145–149 (2006).

29. Cheng, Y., Wang, L. J., Li, J. S., Yang, Y. C. & Sun, X. Y. Preparation and characterization of nanosized ZSM-5 zeolites in the absence of organic template. *Mater. Lett.* **59,** 3427–3430 (2005).

30. Niu, X. *et al.* Influence of crystal size on the catalytic performance of H-ZSM-5 and Zn/H-ZSM-5 in the conversion of methanol to aromatics. *Fuel Process. Technol.* **157,** 99–107 (2017).

31. Raskó, J., Kecskés, T. & Kiss, J. Formaldehyde formation in the interaction of HCOOH with Pt supported on TiO2. *J. Catal.* **224,** 261–268 (2004).

32. Li-Fen Liao, Wen-Chun Wu, Chia-Yuan Chen, and & Lin*, J.-L. Photooxidation of Formic Acid vs Formate and Ethanol vs Ethoxy on TiO2 and Effect of Adsorbed Water on the Rates of Formate and Formic Acid Photooxidation. (2001). doi:10.1021/JP003541J

33. Sápi, A. *et al.* In Situ DRIFTS and NAP-XPS Exploration of the Complexity of CO2 Hydrogenation over Size-Controlled Pt Nanoparticles Supported on Mesoporous NiO. *J. Phys. Chem. C* **122,** 5553–5565 (2018).

34. Novák, É., Fodor, K., Szailer, T., Oszkó, A. & Erdöhelyi, A. CO2 Hydrogenation on Rh/TiO2 Previously Reduced at Different Temperatures. *Top. Catal.* **20,** 107–117 (2002).

35. Wang, X., Shi, H., Kwak, J. H. & Szanyi, J. Mechanism of CO_2 Hydrogenation on Pd/Al_2O_3 Catalysts: Kinetics and Transient DRIFTS-MS Studies. *ACS Catal.* **5,** 6337–6349 (2015).

36. László, B. *et al.* Gold Size Effect in the Thermal-Induced Reaction of CO_2 and H_2 on Titania- and Titanate Nanotube-Supported Gold Catalysts. *J. Nanosci. Nanotechnol.* **19,**

470–477 (2019).

37. Wang, H. *et al.* Dramatically Different Kinetics and Mechanism at Solid/Liquid and Solid/Gas Interfaces for Catalytic Isopropanol Oxidation over Size-Controlled Platinum Nanoparticles. *J. Am. Chem. Soc.* **136,** 10515–10520 (2014).

38. Kiricsi, I., Förster, H., Tasi, G. & Nagy, J. B. Generation, Characterization, and Transformations of Unsaturated Carbenium Ions in Zeolites. *Chem. Rev.* **99,** 2085–2114 (1999).

39. Erdöhelyi, A., Pásztor, M. & Solymosi, F. Catalytic hydrogenation of CO2 over supported palladium. *J. Catal.* **98,** 166–177 (1986).

40. Solymosi, F., Erdöhelyi, A. & Kocsis, M. Surface interaction between H2 and CO2 on RhAl2O3, studied by adsorption and infrared spectroscopic measurements. *J. Catal.* **65,** 428–436 (1980).

41. Román-Martínez, M. C., Cazorla-Amorós, D., Salinas-Martínez de Lecea, C. & Linares-Solano, A. Structure Sensitivity of CO2 Hydrogenation Reaction Catalyzed by Pt/Carbon Catalysts. *Langmuir* **12,** 379–385 (1996).

42. Henderson, M. A. & Worley, S. D. An infrared study of the hydrogenation of carbon dioxide on supported rhodium catalysts. *J. Phys. Chem.* **89,** 1417–1423 (1985).

43. Fisher, I. A. & Bell, A. T. A Comparative Study of CO and CO_2 Hydrogenation over Rh/SiO2. *J. Catal.* **162,** 54–65 (1996).

44. Solymosi, F., Erdöhelyi, A. & Bánsági, T. Infrared study of the surface interaction between H_2 and CO_2 over rhodium on various supports. *J. Chem. Soc. Faraday Trans. 1*

Phys. Chem. Condens. Phases **77,** 2645 (1981).

45. Sachtler, W. M. H. & Ichikawa, M. Catalytic site requirements for elementary steps in syngas conversion to oxygenates over promoted rhodium. *J. Phys. Chem.* **90,** 4752–4758 (1986).

46. Shustorovich, E. & Bell, A. T. Analysis of CO hydrogenation pathways using the bond-order-conservation method. *J. Catal.* **113,** 341–352 (1988).

47. Ferstl, P. *et al.* Adsorption and Activation of CO on Co3O4(111) Thin Films. *J. Phys. Chem. C* **119,** 16688–16699 (2015).

48. Tóth, M. *et al.* Hydrogenation of Carbon Dioxide on Rh, Au and Au–Rh Bimetallic Clusters Supported on Titanate Nanotubes, Nanowires and TiO2. *Top. Catal.* **55,** 747–756 (2012).

49. Chuang, S. S. C., Stevens, R. W. & Khatri, R. Mechanism of C2+ oxygenate synthesis on Rh catalysts. *Top. Catal.* **32,** 225–232 (2005).

50. Ichikawa, M. & Fukushima, T. Infrared studies of metal additive effects on carbon monoxide chemisorption modes on silicon dioxide-supported rhodium-manganese, -titanium and iron catalysts. *J. Phys. Chem.* **89,** 1564–1567 (1985).

51. Stevenson, S. A., Lisitsyn, A. & Knoezinger, H. Adsorption of carbon monoxide on manganese-promoted rhodium/silica catalysts as studied by infrared spectroscopy. *J. Phys. Chem.* **94,** 1576–1581 (1990).

52. Rivallan, M. *et al.* Platinum Sintering on H-ZSM-5 Followed by Chemometrics of CO Adsorption and 2D Pressure-Jump IR Spectroscopy of Adsorbed Species. *Angew. Chemie*

Int. Ed. **49,** 785–789 (2010).

x. Martin, N.M., Velin, P., Skogludh, M., Bauer, M., Carlsson, P-A, Catalytic hydrogenation of CO_2 to methane over Pd Rh, Ni catalysts, Catal. Sci. Technol. **7,** 1086-1094 (2017).